Materials Advances

ROYAL SOCIETY OF CHEMISTRY

PAPER

View Article Online
View Journal | View Issue

Cite this: *Mater. Adv.*, 2021, 2, 2700

Tunable $CsPb(Br/Cl)_3$ perovskite nanocrystals and further advancement in designing light emitting fiber membranes†

Sk Shamim Hasan Abir, [a] Santosh K. Gupta, [bc] A. Ibrahim,[d] Bhupendra B. Srivastava *[d] and Karen Lozano*[a]

Cesium lead halide perovskite nanocrystals (NCs) have drawn a great deal of interest in optoelectronic and photonic applications due to their intrinsic and attractive photoluminescence properties, though, their commercial viability is of concern due to their intrinsic instability. In this study, blue and green luminous PMMA–$CsPbX_3$ (X = Cl/Br) fibers were fabricated *via* the Forcespinning technique, where the polymer matrix encapsulated the NCs. Blue $CsPbX_3$ NCs (b-CPX NCs) were synthesized under ambient conditions while fine color tuned blue to green $CsPbX_3$ NCs (g-CPX NCs) were obtained after heat treatment at 150 °C. Field emission scanning electron microscopy (FESEM) shows fibers with diameters in the single digit microscale. Efficient encapsulation of NCs in the PMMA fiber was confirmed using FTIR spectroscopy. UV visible spectra of the NCs suggested a quantum confinement effect. Pristine NCs show bright blue and green emission from b-CPX and g-CPX NCs under UV irradiation (365 nm) which was successfully reproduced even upon encapsulation in the PMMA matrix. In both cases, the PMMA matrix besides promoting QD encapsulation also enhanced the photoluminescence quantum yield (PLQY) from 25.5% to 31.1% (blue PMMA fibers) and 42.6% to 51.4% (green PMMA fibers) compared to bare NC PLQY. PMMA–$CsPbX_3$ (X = Cl/Br) also possessed narrow half-peak width compared to pristine NCs suggesting high color purity. This work provides a novel polymer fiber-based encapsulation approach to solve the intrinsic instability issues of $CsPbX_3$ NCs, therefore prompting promising practical applications.

Received 3rd March 2021,
Accepted 7th March 2021

DOI: 10.1039/d1ma00183c

rsc.li/materials-advances

1. Introduction

In the last several years inorganic cesium lead halide ($CsPbX_3$, X = Cl, Br and I) perovskites have caught the attention of researchers[1] due to their optoelectronic properties for potential applications in light-emitting devices (LEDs), transistor devices, solar cells, lasers, photo detectors, memory devices, *etc.*[2–9] Their potential arises from their superior photoluminescence quantum yield (PLQY), narrow full width at half maximum (FWHM ~ 20 nm), tunable light emission spanning the full visible spectrum, high defect tolerance *etc.*[10–14] Nevertheless, intrinsic limitations due to their inherent poor stability against moisture, water and low melting temperature owing to their ionic structure and high surface energy pose significant restrictions for adoption in practical applications.[15,16] Moreover, few other issues associated with $CsPbX_3$ NCs such as reduction in PLQY by surface traps and lower thermal stability which can't sustain the junction temperature of the existing light emitting diodes limit their applicability.[17]

In this regard, one of the most widely used methods to protect $CsPbX_3$ NCs is encapsulation within protective matrices, which prevents NCs from agglomeration as well as safeguard them to overcome their thermal and environmental instability.[18] Therefore, several methods such as atomic layer deposition, spin coating, protective coating, nanoparticle coating, synthetic modification, polymer matrix methods, and polymer blend techniques have been applied to enhance the stability of the perovskite nanomaterials and have been pursued to overcome these limitations.[19–24] Nonetheless, the reported studies still face significant challenges to ensure uniform distribution of NCs in matrices, while facing a low production rate, monotonous post-treatment to prepare perovskite materials *etc.* Subsequently, extensive research has been conducted worldwide to find a facile method to avoid the aforementioned shortcomings assuring comprehensive applications of $CsPbX_3$ NCs in optoelectronic fields.

[a] *Department of Mechanical Engineering, University of Texas Rio Grande Valley, Edinburg, TX 78539, USA. E-mail: karen.lozano@utrgv.edu*
[b] *Radiochemistry Division, Bhabha Atomic Research Centre, Trombay, Mumbai-400085, India*
[c] *Homi Bhabha National Institute, Anushakti Nagar, Mumbai-400094, India*
[d] *Department of Chemistry, University of Texas Rio Grande Valley, Edinburg, TX 78539, USA. E-mail: bhupendra.srivastava@utrgv.edu*

† Electronic supplementary information (ESI) available. See DOI: 10.1039/d1ma00183c

Lately, encapsulation of the photoluminescent perovskite NCs in the polymer fiber matrix has drawn significant attention. The making of perovskite composite fine fibers through the electrospinning (ES) technique has been pursued as a potential method to obtain[19,25,26] homogeneous distribution of perovskite NPs given the feasibility to fine-tune fiber diameter and morphology from the nano to microscale.[27–29] Moreover, conjugate polymers, metallic nanoparticles, and perovskite nanocrystals (NCs) can be incorporated in the precursor polymer solution to synthesize fiber composites with higher versatility.[25,27,28,30–32] Polymer matrices besides aiding in preventing agglomeration also provide mechanical and chemical stability to NCs, along with offering processability towards thin films and microsphere structures among other systems. The incorporation of perovskite NCs into fiber structures not only mitigates the aggregation concern but also preserves the pristine inherent properties.[19,26,31,33] In addition, due to the intrinsic geometrical confinement effect, fibers prepared by the electrospinning technique can manipulate the orientation, crystallinity, and optoelectronic properties of the components integrated into the fiber matrix.[25,33–36] Wang *et al.*[33] have encapsulated $CsPbBr_3$ perovskite in PMMA fiber membranes using electrospinning. This method has been proven to overcome many of the abovementioned challenges for the use of NCs, however, electrospinning itself has some shortcomings, such as low yield, high electrostatic forces and a complex, expensive experimental procedure to produce fiber systems.[37–39]

Forcespinning®, a technique used to make fine fiber (nano, submicron and single digit micron scale) systems using centrifugal force, has become an attractive solution to explore fiber systems. Given that electrical fields are not needed, it broadens the choice of materials to be used since dielectric properties are not a factor to be considered.[40,41] Additionally, higher production rates and the ease of processing[42] have prompted attention to this technology to develop fiber membrane systems for a wide variety of applications for example antibacterial gauzes,[43] tissue engineering,[44] air filtration,[45] optical sensors,[46] lithium ion batteries,[47] photoluminescence, *etc.*[48]

In this study we have synthesized blue and green photoluminescent $CsPb(Br/Cl)_3$ perovskite NCs and have used these to develop fine fiber membranes from $CsPb(Br/Cl)_3$/polymer solutions by using the centrifugal spinning method. We used poly(methyl methacrylate) (PMMA) as the polymer matrix. PMMA was chosen because of its good spinnability, high stability, and potential towards surface modification.[49] Photophysical properties such as UV-visible absorption, photoluminescence, and PLQY were investigated. To the authors' knowledge this is the first report on $CsPb(Br/Cl)_3$ perovskite NC luminescent fiber membranes synthesized by the centrifugal spinning technique. By blending the $CsPb(Br/Cl)_3$ perovskite NCs into the PMMA fiber, we observed that fiber systems sustain their spectral emission profile. The encapsulated $CsPb(Cl/Br)_3$ perovskite NCs maintain over 90% of their initial emission intensity under continuous ultraviolet illumination. We could also enhance the PLQY of $CsPb(Cl/Br)_3$ perovskite NCs as well as narrow down the red color emission by encapsulating them inside the PMMA polymer matrix.

2. Experimental

2.1. Materials

Cesium chloride (CsCl, 99.99%), lead(II) bromide ($PbBr_2$, ≥98%), chloroform ($CHCl_3$, ≥99%), toluene (C_7H_8, ≥99%), and *N*,*N*,dimethylformamide (DMF, ≥99.7%) were purchased from Fisher Scientific. Oleyl amine (OA, 70%), oleic acid (OLA, 90%) and polymer poly(methyl methacrylate) (PMMA, M_w = 350 000) were obtained from Sigma Aldrich. All materials were used as received without any further purification.

2.2. Synthesis of $CsPb(Cl/Br_3)$ perovskite NCs

In this work, 0.8 mmol of CsCl and 0.8 mmol of $PbBr_2$ were added in 10 mL of DMF to synthesize $CsPb(Cl/Br)_3$ solutions. Afterwards, 1 mL of OLA and 1 mL of OA were added to stabilize the precursor solution. Subsequently, the solution was vortexed for 5 minutes to obtain blue luminescence NCs at room temperature whereas the stabilized solution was heated at 150 °C for 15 minutes at 600 rpm using a magnetic stirrer to synthesize green luminescence NCs. Aliquot of the stock solution was added in toluene to check photoluminescence under UV light. Later, this stock solution was transferred into a centrifuge test tube to wash it with acetone and NCs were collected by centrifuging the solution at 700 rpm for 10 minutes. NCs were then dispersed into chloroform. Furthermore, two more cycles of precipitation and dispersion were repeated using acetone/chloroform. Finally the washed sample was again re-dispersed in chloroform. The final washed sample is abbreviated as b-CPX NCs and g-CPX NCs for blue and green emitting $CsPb(Cl/Br)_3$ perovskite NCs, respectively. Fig. 1 shows the schematic of blue and green emitting $CsPb(Cl/Br)_3$ perovskite-b-CPX and g-CPX NCs.

2.3. Preparation of NP encapsulated PMMA fibers

In order to prepare the polymer solution, PMMA was added to NP embedded chloroform solution in a 20 mL glass vial to make 13 wt% polymer solutions. The solution was then mechanically stirred using magnetic stirring at room temperature for 12 h at 700 rpm to ensure complete dissolution. Afterwards, 2 mL of the thick viscous solution were injected into the Cyclone (Fiberio Technology Inc.) spinneret equipped with a 30-gauge half inch regular needle. The solution was subjected to 5000 rpm for 2 minutes, and the developed fibers were deposited on eight prolonged metal collectors, collected in a nonwoven fashion, and stored in HDPE bags containing silica desiccant. The developed systems will be known as b-CPX:F and g-CPX:F for blue and green emitting $CsPb(Cl/Br)_3$ perovskite NC encapsulated PMMA fibers respectively.

2.4. Characterization

The synthesized NCs and developed fiber membranes were analyzed using an X-ray diffractometer (XRD). Powder XRD

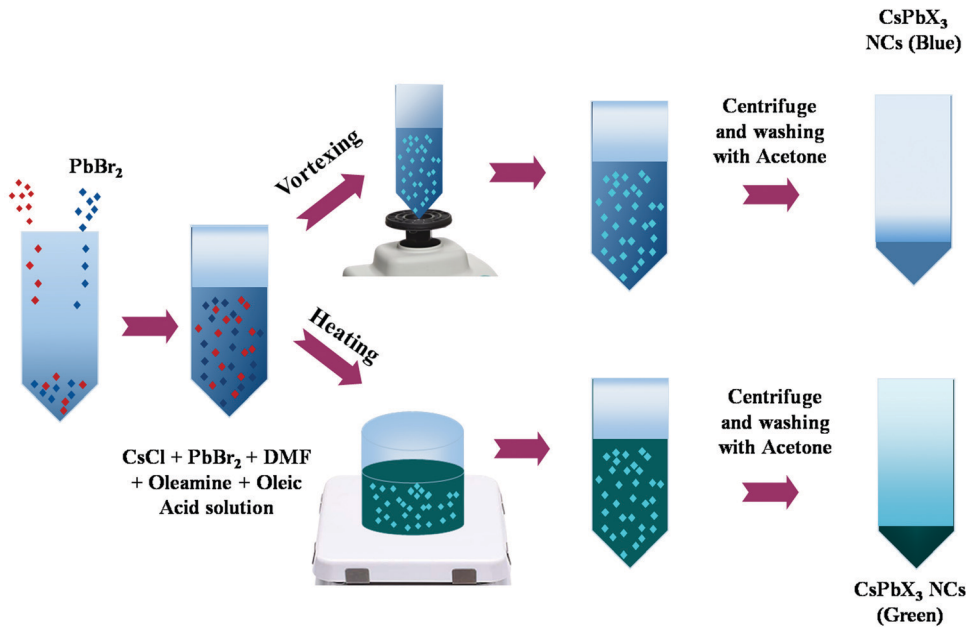

Fig. 1 Schematic for the synthesis of b-CPX NCs and g-CPX NCs.

patterns of the nanoparticles and fine fibers were recorded using a Bruker D8 Advance X-ray diffractometer (XRD) with Cu Kα1 radiation (λ = 0.15406 nm). The XRD data were collected using a scanning mode of 2θ with a scanning step size of 0.04° and a scanning rate of 2.0° min^{-1}. The morphology of the CsPb(Cl/Br)$_3$ perovskite NCs and the corresponding fibers were characterized using a field emission scanning electron microscope (FESEM) which was kept at an acceleration voltage of 1.0 kV (Sigma VP, Carl Zeiss, Jena, Germany). The Fourier Transform Infrared Spectra of the CsPb(Cl/Br)$_3$ perovskite NCs and the corresponding fibers were obtained using a 133 VERTEX 70v FTIR Spectrometer (Bruker) in an Attenuated Total Reflection (ATR) mode. Photoluminescence emissions were measured using an Edinburgh Instrument FLS 980 fluorimeter with a steady state xenon lamp source. A 150 mm BenFlect coated integrating sphere was used to determine the absolute quantum yield (QY) of the NPs. The spectral sensitivity of the spectrometer and the sphere was modified using a calibrated lamp for spectral light throughput.

3. Results and discussion

3.1. X-ray diffraction

Fig. 2 shows the XRD patterns of the CsPb(Cl/Br)$_3$ perovskite NCs and fiber. Fig. 2a shows the XRD pattern of b-CPX NCs; the observed peaks match well with that of the cubic CsPbBr$_3$ structure corresponding to JCPDS number 54-0752 therefore confirming the formation of a pure compound.[50] These also suggest that CsPb(Cl/Br)$_3$ has a similar structure to CsPbBr$_3$. As shown in Fig. 2b for g-CPX-NCs, all of the diffraction peaks are slightly shifted to a lower 2θ value compared to cubic b-CPX NCs (space group *Pm*3*m*, PDF#73-0692). This could be ascribed

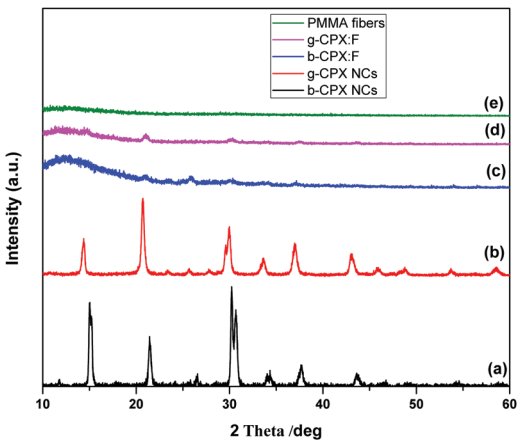

Fig. 2 XRD patterns of (a) b-CPX NCs, (b) g-CPX NCs, (c) b-CPX:F, (d) g-CPX:F and (e) PMMA fiber.

to the thermally induced effect of b-CPX NCs, causing expansion in the unit cell and lower angle shifting of the peaks. The same could also be ascribed to variation in the Cl/Br ratio on 150 °C heated sample of g-CPX-NCs. PMMA masks XRD for the forcespun NC loaded fibers particularly in the lower 2θ range, however the presence of NCs is observable at the highest peaks similar to bare NCs (Fig. 2c and d). This suggested that the intrinsic cubic structure of NCs is retained even on encapsulation in the PMMA matrix as fibers. The broad peak in the 10–20° range is typical of the PMMA polymer (Fig. 2e).

3.2. TEM investigations on CsPb(Cl/Br)$_3$ perovskite NCs and the corresponding fibers

Fig. 3a–d shows the TEM images of CsPbX$_3$ perovskite. The image shown in Fig. 3a and b is for b-CPX NCs and that

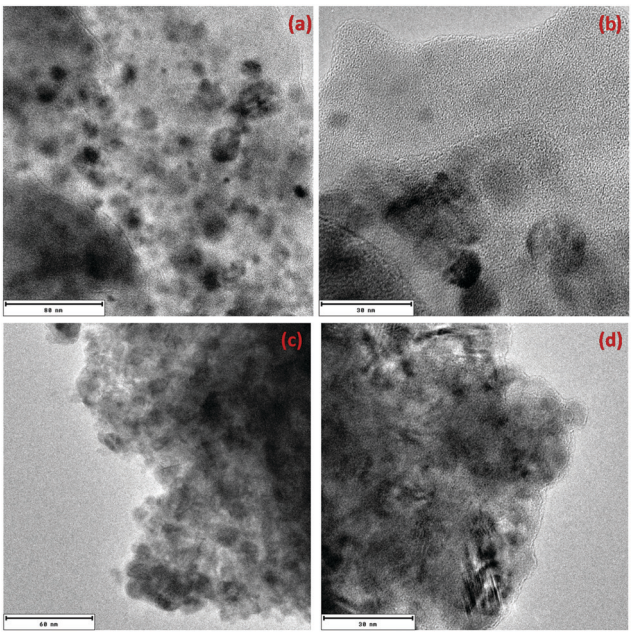

Fig. 3 TEM images of (a and b) b-CPX and (c and d) g-CPX NCs.

shown in Fig. 3c and d is for g-CPX at different magnifications. It is clearly seen from Fig. 3a and b that the b-CPX perovskite has nanodimension of 20–30 nm with very high monodispersity and uniform dispersion. They seem to stabilize in an aggregate free domain. The shape of the NCs seems more like a sphere. The stabilization of aggregate free NCs in chloroform is explained by the fact that coulombic interactions among nanocrystallites in the b-CPX perovskite could overcome the van der Waals forces. The similar morphological evolution was also seen for the g-CPS perovskite (Fig. 3c and d). The size is almost of a similar range but there is slight enhancement in the degree of aggregation owing to thermal treatment at 150 °C. The shape and texture though remained the same.

3.3. Morphology of PMMA and NC loaded fibers

Fig. 4a–c shows the FESEM micrographs of pristine PMMA and b-CPX:F and g-CPX:F fibers. The developed fiber systems show an average diameter of ~2.8 and 3.0 micron respectively. The pristine unloaded PMMA fiber was found to have an average diameter of ~2.7 micron; suggesting enhancement in the fiber diameter upon NC encapsulation. PMMA and b-CPX:F (Fig. 4a and b) show long, continuous fibers with smooth surface texture while the g-CPX:F fibers present a rough surface (Fig. 4c). Broadly both b-CPX:F and g-CPX:F fibers do not display NC aggregates on their surface and the cross sections of the fibers display uniformity. The developed fiber system shows the absence of beads and other surface defects/cracks which are commonly observed as instabilities arising from inadequate balance among surface tension/charge density.[51,52] Several other SEM images at different magnification for PMMA, b-CPX:F and g-CPX:F systems are shown in Fig. S1–S3 (ESI†), respectively. We have also carried out energy dispersive X-ray (EDX) measurements (Fig. S4, ESI†) on one of the representative b-CPX:F samples to show our efficient method for preparing $CsPbX_3$ NCs encapsulated inside the PMMA polymeric fiber. The representative EDX spectrum shows the presence of X-ray lines of C, O, Cs, Pb and Cl/Br ions. Elemental mapping (Fig. S5, ESI†) clearly shows uniform distribution of the nanocrystals inside the PMAA polymeric fiber matrix.

3.4. Vibration features of $CsPbX_3$ perovskite NCs and the corresponding fibers

The FT-IR spectrum is shown in Fig. 5. This spectrum displays weaker broad peaks at around ~3400 cm^{-1} particularly for bare NCs (b-CPX NCs and g-CPX NCs) corresponding to –OH stretching of the carboxylic group of oleic acid. Importantly, the characteristic C–H stretching vibrations at 2800–3000 cm^{-1} in NCs are derived from the long hydrocarbon chain portion of OA and OLA on the surface of NCs.[53,54] The other peak at 2925 cm^{-1} corresponds to –N–H stretching of OA; 2856 cm^{-1} corresponds to the asymmetric stretching of CH_3. The peak around 1450 cm^{-1} is attributed to $-NH_2/-COO^-$ vibration arising out of the amine/carboxylic acid group.[53,54] Interestingly, the intensity of the entire peak in the range of 2800–3000 cm^{-1} reduces for the g-CPX NCs. This is attributed to heating induced changes which occurred at 150 °C for g-CPX NCs. The features in the lower wavelength region around 750–900 cm^{-1} are typical lead–halogen bonds (Pb–X) predominantly present in g-CPX NCs and b-CPX NCs (black and red spectra). These NC bands are completely masked when encapsulated within the polymer (blue and green spectra). A sharp and very intense IR peak at around 1730 cm^{-1} is ascribed to the ester carbonyl group stretching vibration.[55] The IR band spanning 1250–1000 cm^{-1} is attributed to the C–O (ester bond) stretching vibration.[33] The broad IR band in the range of 950–650 cm^{-1} is mainly because of C–H bending whereas the peak in the range of 3100–2900 cm^{-1} is due to the presence of the CH stretching vibration of PMMA.[55]

3.5. Optical properties of $CsPbX_3$ perovskite NCs and the corresponding fibers

The optical properties of the $CsPbX_3$ perovskite NCs and the corresponding fibers were studied by measuring ultraviolet and visible absorption (UV-vis) and photoluminescence (PL) spectra. Fig. 6a shows the UV-vis spectra of b-CPX NCs and b-CPX:F. The absorption peak of the b-CPX-NCs is around 424 nm. This band is typical of exciton absorption causing electronic transition from the valence band maxima to the conduction band minima. The heating of b-CPX-NCs at 150 °C further causes a substantial red shift of the absorption band to 460 nm in g-CPX NCs (Fig. 6b, black spectra) leading to reduction in the band gap. In general, the band gap of the material is affected significantly by electron–phonon interactions (EPIs) and thermal expansion behavior (TEB).[56] The former mostly leads to a red shift in the band gap whereas a blue shift is mostly triggered by TEB. There can be an opposite trend in the band gap for the case of two phonon modes wherein two effects counter balance each other.[57] Here in this case thermally induced reduction in the band gap is ascribed to an increase in the coefficient of thermal expansion with an increase in temperature. This leads to band gap narrowing and

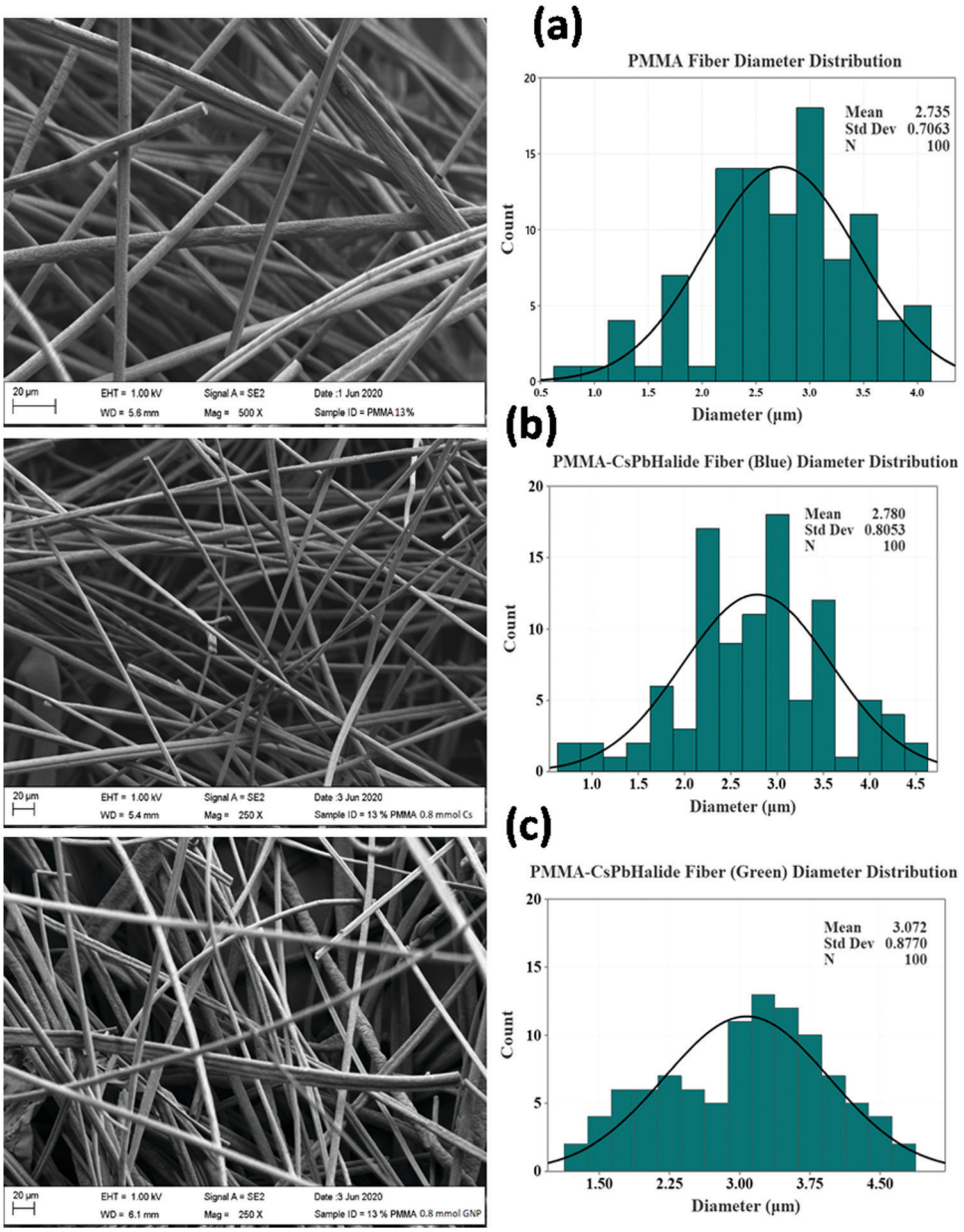

Fig. 4 FESEM micrographs and size distribution histograms of (a) PMMA fiber, (b) b-CPX: F and (c) g-CPX: F.

hence a red shift in exciton absorption maxima. A similar phenomenon has been seen in $CH_3NH_3PbI_{3-x}Cl_x$ films.[58] The absorption band is slightly red shifted from 424 nm to 427 nm after encapsulation in the PMMA fiber in the case of b-CPX-F with significant reduction in intensity (Fig. 6a, red spectra). A similar spectral shift is observed in the absorption band of g-CPX NCs after encapsulation in PMMA but not much change in intensity could be seen in this case (Fig. 6b, red spectra).

Digital images under daylight and UV light for b-CPX:F are shown in Fig. 7a and c, respectively. It can be clearly seen that fiber systems display bright blue emission under UV light irradiation. The corresponding emission spectra of NCs and fibers (b-CPX NCs and b-CPX:F) at 365 nm are shown in Fig. 7b. The emission spectra of b-CPX NCs depicted a blue band located around 469 nm (navy blue spectra). This narrow blue band emission positioned at 469 nm with a FWHM of 16 nm is assigned to the $CsPb(Cl/Br)_3$ host involving band to band transition. Interestingly this peak narrows down with a FWHM of 14 nm and exhibited a red shift to 474 nm on encapsulation inside the PMMA fiber (blue spectra). This could be attributed to loading of bigger NPs from the ensemble or size enhancement fractionally in the force spun PMMA fiber. The b-CPX solution in chloroform also displayed bright blue luminescence under UV illumination which could be useful in bioimaging (inset of Fig. 7c).

Digital images in daylight and under UV light for g-CPX:F are shown in Fig. 8a and c respectively. It can be clearly seen that the fiber displayed bright green emission under UV light

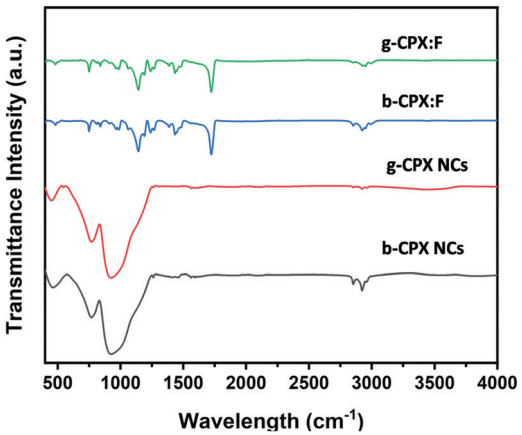

Fig. 5 FTIR spectra of $CsPb(Cl/Br)_3$ perovskite NCs and the corresponding fibers.

irradiation. So just by heating the as prepared b-CPX NCs at 150 °C we can tune the color emitted by NCs from bright blue to bright green as can be seen in the digital image of fiber and solution under UV excitation (Fig. 8b and inset of Fig. 8c). The corresponding emission spectra of NCs and fibers (g-CPX NCs and g-CPX:F) at 365 nm are shown in Fig. 8b. The emission spectra of g-CPX NCs depicted a green band located around 469 nm (navy blue spectra). This narrow blue band emission positioned at 487 nm with FWHM 13 nm is assigned to the $CsPb(Cl/Br)_3$ host involving the band to band transition similar to a previous case. Interestingly, here in this case as well the peak narrows down to a much lower value with a FWHM of 8 nm and exhibited a red shift to 490 nm on encapsulation inside the PMMA fiber (blue spectra). This small red-shift and narrowing down of the peak width after the formation of force-spun fibers compared to bare NPs suggest that mostly larger particles from the nanoparticle ensemble load during force spin formation. So, we can clearly pin point the fact that encapsulating the NCs in the fiber improves the color purity significantly which can be of great relevance in designing efficient light emitting materials. The emission spectra of pristine PMMA do not show prominent features which could be attributed to the lack of a crystalline field and a large organic moiety (violet spectra in both Fig. 7b and 8b).

In both absorption and emission spectra of b-CPX:F and g-CPX:F, there is a red shift in the peak position. The dielectric constant of chloroform, $CsPbX_3$ and PMMA is 4.81, 6.1 and 3.0 respectively. Hu *et al.* have pointed out that comparable dielectric constants of off-stoichiometry thiol–ene (OSTE) and $CsPbX_3$ NCs suppress the dielectric screen effect and reduce the exciton binding energies, leading to a blueshift of PL peak positions.[59] In contrast we observe a red shift in the PL band which was attributed to a large difference in the dielectric constant of $CsPbX_3$ and PMMA polymers inducing enhancement in the dielectric screen effect and an increase in the exciton binding energies, leading to a red shift of PL peak positions. Moreover, the encapsulation of $CsPbX_3$ NCs inside the PMMA polymeric fiber will enhance the photon recycling and photon reabsorption, which may also lead to a red-shifted PL peak position.[60,61]

Also there is narrowing down of the PL band in the case of fibers compared to bare nanocrystals. The peak narrowing is ascribed to reduced electron–phonon interactions when NCs are encapsulated inside the PMMA fiber. This is due to the soft polymer encapsulation weakening of crystal-field strength, leading to the larger band splitting; and reduced electron–phonon coupling and hence a decrease in full width half maxima (FWHM) of the emission band is seen. Though Hu *et al.* have observed an increase in FWHM when $CsPbX_3$ NCs ar encapsulated inside OSTE. It is expected that the force spun PMMA fiber behaves differently from OSTE.

To further corroborate our results, we have also calculated PLQY (both absolute and relative) employing an integrating sphere and the obtained value is listed in Table 1. The QY of g-CPX and b-CPX NCs was also measured relative to fluorescein isothiocyanate (FITC) (QY 92% in 0.1 N NaOH) with excitation at 492 nm. Fluorescence spectra of NPs and dyes were taken under identical spectrometer conditions in triplicate and averaged. Solutions were degassed with argon in the cuvettes. The optical density was kept below 0.1 at the maximum excitation.

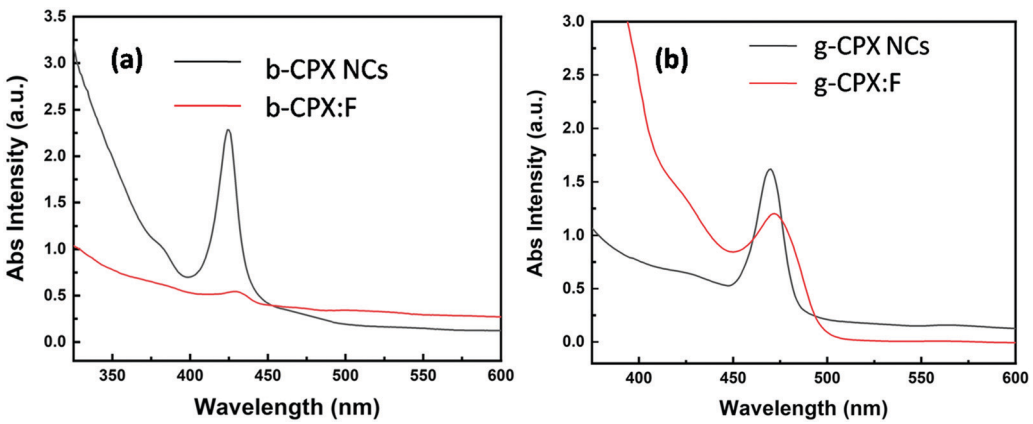

Fig. 6 UV Visible spectra of (a) b-CPX NCs and b-CPX:F and (b) g-CPX NCs and g-CPX:F.

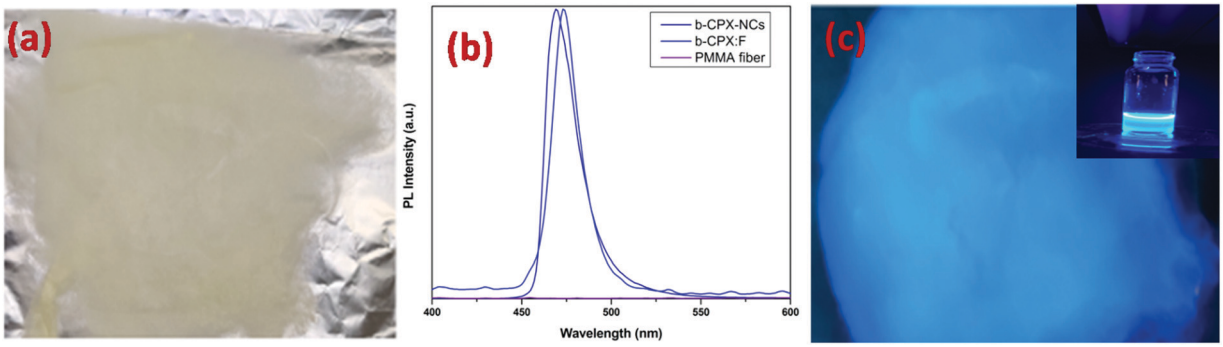

Fig. 7 (a) b-CPX-F in day light, (b) PL emission spectra of b-CPX NCs, b-CPX-F and PMMA fiber and (c) b-CPX-F under UV light. The inset of c shows the digital image of b-CPX NC solution under UV light.

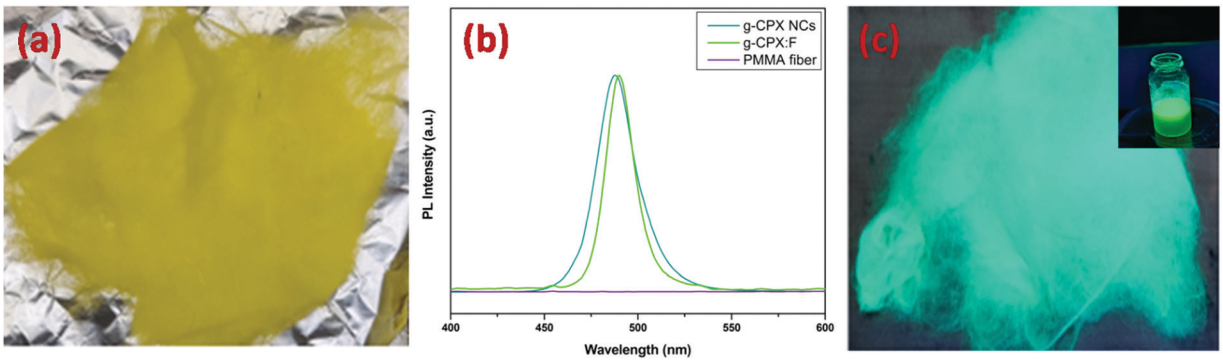

Fig. 8 (a) g-CPX-F in day light, (b) PL emission spectra of g-CPX NCs, g-CPX-F and PMMA fiber and (c) g-CPX-F under UV light. The inset of Fig. 7c shows the digital image of g-CPX NC solution under UV light.

Table 1 PLQY values for $CsPb(Cl/Br)_3$ perovskite NCs and the corresponding fibers

Sample name	Absolute method for QY (%)	Dye comparison method for QY (%)
b-CPX NCs	25.5	25.8
b-CPX:F	31.1	—
g-CPX NCs	42.6	45.9
g-CPX:F	51.4	—

The details of calculations are mentioned as I1 (ESI†) and the corresponding plots are shown in Fig. S6 and S7 which consist of UV-visible, photoluminescence spectra and a plot of optical density *versus* emission area using different concentrations of the dye fluorescein isothiocyanate (FITC) solution (0.1 N NaOH) and our g-CPX and b-CPX NCs.

It can be seen clearly from Table 1 that well dispersed NCs in PMMA polymeric fibers enhanced QY (31.1% for b-CPX:F and 51.4% for g-CPX:F) compared to bare ones (25.5% for b-CPX NCs and 42.6% for g-CPX NCs). The same has been attributed to the uniform and homogeneous distribution of NCs in the PMMA fiber. This again shows the advantage of encapsulating $CsPbX_3$ perovskite NCs inside the polymer matrix in the form of a fine fiber. We have also carried out PL measurements for fiber samples at different UV exposure times and different time durations throughout the day to check its photostability. The PL emission spectra of both blue and green fibers after UV irradiation for 1, 2, 4, 8, 12 and 24 h are shown in Fig. S8 (ESI†). The samples were quite photostable with not much changes seen in the emission spectra. Though slight intensity enhancement at higher exposure time was observed it may be attributed to the generation of defects mostly oxygen vacancies. The radiative enhancement was ascribed to the recombination of photoexcited holes and electrons trapped in oxygen vacancies.

Direct moisture measurement was difficult to perform due to large OH density which quenches the fluorescence significantly as UTRGV is located in the southern part of Texas with varying humid conditions throughout the day. The PL emission spectra of both blue and green fibers at different time durations throughout the day to sense different moist conditions are shown in Fig. S9 (ESI†). Again the sample doesn't depict much change in the PL emission profile throughout the day right from early morning to night. The samples were quite photostable with not much changes seen in the emission spectra.

Fig. 9 shows the entire crux of this work showing synthesis of NCs, encapsulation in the PMMA fiber using Forcespinning and their bright blue and green PL emission under UV irradiation.

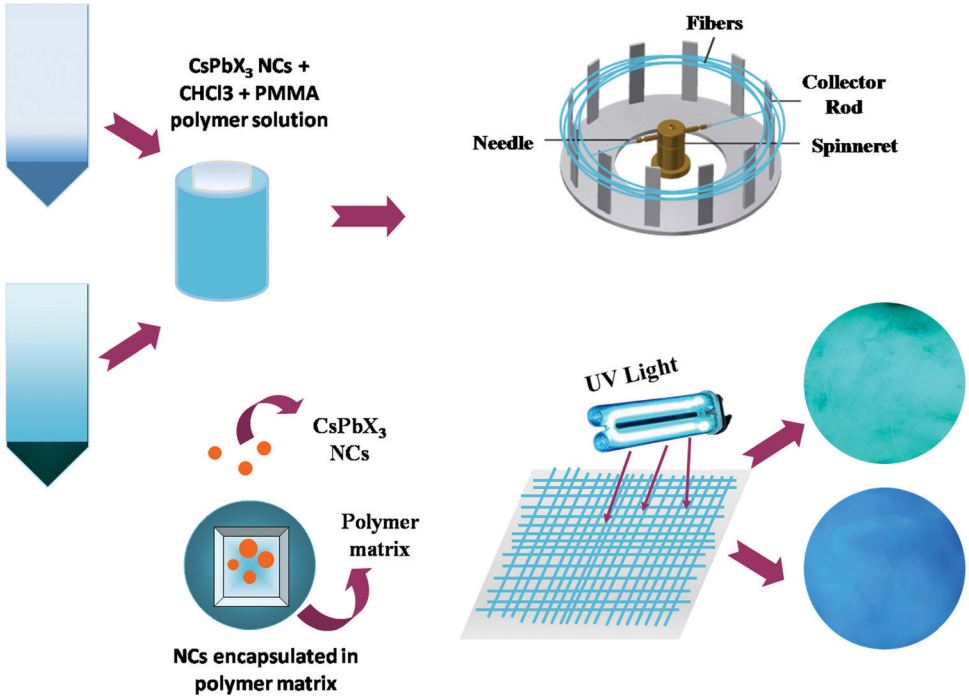

Fig. 9 Schematic showing the synthesis of NCs, encapsulation in PMMA, forcespinning and bright PL under UV.

4. Conclusions

In summary, we demonstrated for the first time, the development of $CsPbX_3$(X = Cl/Br) perovskite NC embedded PMMA luminescent fibers through the Forcespinning® method. The color tunability from blue to green was achieved upon heat treatment probably due to an increase of NC size. The inclusion of NCs in the fiber matrix resulted in single digit micron fibers. FTIR suggested the formation of NCs as well as their efficient encapsulation within the PMMA matrix. In both cases, the encapsulation of NCs in fiber matrices resulted in the absorption band red shifted due to the quantum confinement effect. Similar results were also noticed in the case of PL emission spectra where the band spectra shifted from 469 (b-CPX:NCs) to 474 nm (b-CPX:F) and 487 (g-CPX:NCs) to 490 nm (g-CPX:F). The PLQY characteristics were not only retained in the fibers but also surpassed the bare NCs which highlighted the homogeneous distribution of the NCs within the PMMA fiber. PMMA–$CsPbX_3$ (X = Cl/Br) also possessed a narrow half-peak width compared to pristine NCs suggesting high color purity. It should be mentioned here that it is very difficult to determine the exact ratio of Cl/Br in the $CsPb(Cl/Br)_3$NC@fiber because of developed interfaces within the fiber system. Future work needs to devise an efficient approach to determine the Cl/Br ratio to have much more control on color emission. This finding reveals that the Forcespinning® technique is a potential alternative for developing perovskite photoluminescence fiber systems with intense blue and green photoluminescence under UV light. The present work may open up a new way for multicolor fluorescent $CsPbX_3$ fiber fabrication and more importantly color tunability under ambient conditions.

Conflicts of interest

There are no conflicts to declare.

Acknowledgements

This research was supported by the NSF PREM award under grant No. DMR-1523577: UTRGV-UMN Partnership for Fostering Innovation by Bridging Excellence in Research and Student Success. The authors would like to thank Dr. Ana Stevanovic (Kleberg Advanced Microscopy Center, University of Texas at San Antonio) for helping with TEM imaging.

References

1 A. Kojima, K. Teshima, Y. Shirai and T. Miyasaka, Organometal halide perovskites as visible-light sensitizers for photovoltaic cells, *J. Am. Chem. Soc.*, 2009, **131**, 6050–6051.
2 E. Ercan, J. Y. Chen, P. C. Tsai, J. Y. Lam, S. C. W. Huang, C. C. Chueh and W. C. Chen, A Redox-Based Resistive Switching Memory Device Consisting of Organic–Inorganic Hybrid Perovskite/Polymer Composite Thin Film, *Adv. Electron. Mater.*, 2017, **3**, 1700344.
3 E. Ercan, J.-Y. Chen, C.-C. Shih, C.-C. Chueh and W.-C. Chen, Influence of polymeric electrets on the performance of derived hybrid perovskite-based photo-memory devices, *Nanoscale*, 2018, **10**, 18869–18877.
4 H.-S. Kim, C.-R. Lee, J.-H. Im, K.-B. Lee, T. Moehl, A. Marchioro, S.-J. Moon, R. Humphry-Baker, J.-H. Yum and J. E. Moser, Lead iodide perovskite sensitized

all-solid-state submicron thin film mesoscopic solar cell with efficiency exceeding 9%, *Sci. Rep.*, 2012, **2**, 1–7.

5 X. Li, Y. Wu, S. Zhang, B. Cai, Y. Gu, J. Song and H. Zeng, $CsPbX_3$ quantum dots for lighting and displays: room-temperature synthesis, photoluminescence superiorities, underlying origins and white light-emitting diodes, *Adv. Funct. Mater.*, 2016, **26**, 2435–2445.

6 J. Y. Oh, S. Rondeau-Gagné, Y.-C. Chiu, A. Chortos, F. Lissel, G.-J. N. Wang, B. C. Schroeder, T. Kurosawa, J. Lopez and T. Katsumata, Intrinsically stretchable and healable semiconducting polymer for organic transistors, *Nature*, 2016, **539**, 411–415.

7 J. Song, J. Li, X. Li, L. Xu, Y. Dong and H. Zeng, Quantum dot light-emitting diodes based on inorganic perovskite cesium lead halides (CsPbX3), *Adv. Mater.*, 2015, **27**, 7162–7167.

8 S. Yakunin, L. Protesescu, F. Krieg, M. I. Bodnarchuk, G. Nedelcu, M. Humer, G. De Luca, M. Fiebig, W. Heiss and M. V. Kovalenko, Low-threshold amplified spontaneous emission and lasing from colloidal nanocrystals of caesium lead halide perovskites, *Nat. Commun.*, 2015, **6**, 1–9.

9 Y. Zhang, D. J. Hellebusch, N. D. Bronstein, C. Ko, D. F. Ogletree, M. Salmeron and A. P. Alivisatos, Ultrasensitive photodetectors exploiting electrostatic trapping and percolation transport, *Nat. Commun.*, 2016, **7**, 1–9.

10 Q. A. Akkerman, V. D'Innocenzo, S. Accornero, A. Scarpellini, A. Petrozza, M. Prato and L. Manna, Tuning the optical properties of cesium lead halide perovskite nanocrystals by anion exchange reactions, *J. Am. Chem. Soc.*, 2015, **137**, 10276–10281.

11 W. Chen, J. Hao, W. Hu, Z. Zang, X. Tang, L. Fang, T. Niu and M. Zhou, Enhanced stability and tunable photoluminescence in perovskite $CsPbX_3$/ZnS quantum dot heterostructure, *Small*, 2017, **13**, 1604085.

12 J. B. Hoffman, A. L. Schleper and P. V. Kamat, Transformation of sintered $CsPbBr_3$ nanocrystals to cubic $CsPBI_3$ and gradient $CsPbBr_xI_{3-x}$ through halide exchange, *J. Am. Chem. Soc.*, 2016, **138**, 8603–8611.

13 L. Protesescu, S. Yakunin, M. I. Bodnarchuk, F. Krieg, R. Caputo, C. H. Hendon, R. X. Yang, A. Walsh and M. V. Kovalenko, Nanocrystals of cesium lead halide perovskites (CsPbX3, X= Cl, Br, and I): novel optoelectronic materials showing bright emission with wide color gamut, *Nano Lett.*, 2015, **15**, 3692–3696.

14 M. C. Weidman, M. Seitz, S. D. Stranks and W. A. Tisdale, Highly tunable colloidal perovskite nanoplatelets through variable cation, metal, and halide composition, *ACS Nano*, 2016, **10**, 7830–7839.

15 M. Grätzel, The light and shade of perovskite solar cells, *Nat. Mater.*, 2014, **13**, 838–842.

16 B. Hailegnaw, S. Kirmayer, E. Edri, G. Hodes and D. Cahen, Rain on methylammonium lead iodide based perovskites: possible environmental effects of perovskite solar cells, *J. Phys. Chem. Lett.*, 2015, **6**, 1543–1547.

17 X. Zhang, H.-C. Wang, A.-C. Tang, S.-Y. Lin, H.-C. Tong, C.-Y. Chen, Y.-C. Lee, T.-L. Tsai and R.-S. Liu, Robust and Stable Narrow-Band Green Emitter: An Option for Advanced Wide-Color-Gamut Backlight Display, *Chem. Mater.*, 2016, **28**, 8493–8497.

18 H. Liao, S. Guo, S. Cao, L. Wang, F. Gao, Z. Yang, J. Zheng and W. Yang, A General Strategy for In Situ Growth of All-Inorganic CsPbX3 (X= Br, I, and Cl) Perovskite Nanocrystals in Polymer Fibers toward Significantly Enhanced Water/Thermal Stabilities, *Adv. Opt. Mater.*, 2018, **6**, 1800346.

19 J. Hai, H. Li, Y. Zhao, F. Chen, Y. Peng and B. Wang, Designing of blue, green, and red CsPbX 3 perovskite-codoped flexible films with water resistant property and elimination of anion-exchange for tunable white light emission, *Chem. Commun.*, 2017, **53**, 5400–5403.

20 H. Huang, B. Chen, Z. Wang, T. F. Hung, A. S. Susha, H. Zhong and A. L. Rogach, Water resistant CsPbX 3 nanocrystals coated with polyhedral oligomeric silsesquioxane and their use as solid state luminophores in all-perovskite white light-emitting devices, *Chem. Sci.*, 2016, **7**, 5699–5703.

21 Z. Li, L. Kong, S. Huang and L. Li, Highly luminescent and ultrastable CsPbBr3 perovskite quantum dots incorporated into a silica/alumina monolith, *Angew. Chem.*, 2017, **129**, 8246–8250.

22 A. Loiudice, S. Saris, E. Oveisi, D. T. Alexander and R. Buonsanti, CsPbBr3 QD/AlOx inorganic nanocomposites with exceptional stability in water, light, and heat, *Angew. Chem., Int. Ed.*, 2017, **56**, 10696–10701.

23 S. N. Raja, Y. Bekenstein, M. A. Koc, S. Fischer, D. Zhang, L. Lin, R. O. Ritchie, P. Yang and A. P. Alivisatos, Encapsulation of perovskite nanocrystals into macroscale polymer matrices: enhanced stability and polarization, *ACS Appl. Mater. Interfaces*, 2016, **8**, 35523–35533.

24 Q. Zhou, Z. Bai, W. G. Lu, Y. Wang, B. Zou and H. Zhong, *In situ* fabrication of halide perovskite nanocrystal-embedded polymer composite films with enhanced photoluminescence for display backlights, *Adv. Mater.*, 2016, **28**, 9163–9168.

25 P. C. Tsai, J. Y. Chen, E. Ercan, C. C. Chueh, S. H. Tung and W. C. Chen, Uniform Luminous Perovskite Nanofibers with Color-Tunability and Improved Stability Prepared by One-Step Core/Shell Electrospinning, *Small*, 2018, **14**, 1704379.

26 Y. Wang, Y. Zhu, J. Huang, J. Cai, J. Zhu, X. Yang, J. Shen, H. Jiang and C. Li, CsPbBr3 perovskite quantum dots-based monolithic electrospun fiber membrane as an ultrastable and ultrasensitive fluorescent sensor in aqueous medium, *J. Phys. Chem. Lett.*, 2016, **7**, 4253–4258.

27 D.-H. Jiang, P.-C. Tsai, C.-C. Kuo, F.-C. Jhuang, H.-C. Guo, S.-P. Chen, Y.-C. Liao, T. Satoh and S.-H. Tung, Facile preparation of Cu/Ag core/shell electrospun nanofibers as highly stable and flexible transparent conductive electrodes for optoelectronic devices, *ACS Appl. Mater. Interfaces*, 2019, **11**, 10118–10127.

28 C. C. Kuo, C. T. Wang and W. C. Chen, Highly-Aligned Electrospun Luminescent Nanofibers Prepared from Polyfluorene/PMMA Blends: Fabrication, Morphology, Photophysical Properties and Sensory Applications, *Macromol. Mater. Eng.*, 2008, **293**, 999–1008.

29 D. Li, Y. Wang and Y. Xia, Electrospinning nanofibers as uniaxially aligned arrays and layer-by-layer stacked films, *Adv. Mater.*, 2004, **16**, 361–366.
30 H. Jeong and J. K. Lee, Organic–Inorganic Hybrid Ternary Bulk Heterojunction of Nanostructured Perovskite–Low Bandgap Polymer–PCBM for Improved Efficiency of Organic Solar Cells, *ACS Appl. Mater. Interfaces*, 2015, **7**, 28459–28465.
31 C. C. Lin, D.-H. Jiang, C.-C. Kuo, C.-J. Cho, Y.-H. Tsai, T. Satoh and C. Su, Water-resistant efficient stretchable perovskite-embedded fiber membranes for light-emitting diodes, *ACS Appl. Mater. Interfaces*, 2018, **10**, 2210–2215.
32 P. Wang, L. Zhang, Y. Xia, L. Tong, X. Xu and Y. Ying, Polymer nanofibers embedded with aligned gold nanorods: a new platform for plasmonic studies and optical sensing, *Nano Lett.*, 2012, **12**, 3145–3150.
33 Y. Wang, Y. Zhu, J. Huang, J. Cai, J. Zhu, X. Yang, J. Shen and C. Li, Perovskite quantum dots encapsulated in electrospun fiber membranes as multifunctional supersensitive sensors for biomolecules, metal ions and pH, *Nanoscale Horiz.*, 2017, **2**, 225–232.
34 J.-Y. Chen, H.-C. Hsieh, Y.-C. Chiu, W.-Y. Lee, C.-C. Hung, C.-C. Chueh and W.-C. Chen, Electrospinning-induced elastomeric properties of conjugated polymers for extremely stretchable nanofibers and rubbery optoelectronics, *J. Mater. Chem. C*, 2020, **8**, 873–882.
35 Y.-W. Lin, C.-J. Lin, Y.-H. Chou, C.-L. Liu, H.-C. Chang and W.-C. Chen, Nonvolatile organic field effect transistor memory devices using one-dimensional aligned electrospun nanofiber channels of semiconducting polymers, *J. Mater. Chem. C*, 2013, **1**, 5336–5343.
36 P. Viswanathamurthi, N. Bhattarai, H. Y. Kim and D. R. Lee, The photoluminescence properties of zinc oxide nanofibres prepared by electrospinning, *Nanotechnology*, 2003, **15**, 320.
37 H. L. Schreuder-Gibson and P. Gibson, *Applications of electrospun nanofibers in current and future materials*, ACS Publications, 2006.
38 F. L. Zhou, R. H. Gong and I. Porat, Polymeric nanofibers via flat spinneret electrospinning, *Polym. Eng. Sci.*, 2009, **49**, 2475–2481.
39 X. Shi, W. Zhou, D. Ma, Q. Ma, D. Bridges, Y. Ma and A. Hu, Electrospinning of nanofibers and their applications for energy devices, *J. Nanomater.*, 2015, 122.
40 K. Sarkar, C. Gomez, S. Zambrano, M. Ramirez, E. de Hoyos, H. Vasquez and K. Lozano, Electrospinning to forcespinning™, *Mater. Today*, 2010, **13**, 12–14.
41 X. Zhang and Y. Lu, Centrifugal spinning: an alternative approach to fabricate nanofibers at high speed and low cost, *Polym. Rev.*, 2014, **54**, 677–701.
42 G. Bhat, Polymeric nanofibers: recent technology advancements stimulating their growth, *J. Text. Sci. Eng.*, 2015, **5**, 2.
43 M. Akia, C. Rodriguez, L. Materon, R. Gilkerson and K. Lozano, Antibacterial activity of polymeric nanofiber membranes impregnated with Texas sour orange juice, *Eur. Polym. J.*, 2019, **115**, 1–5.
44 M. Akia, N. Salinas, C. Rodriguez, R. Gilkerson, L. Materon and K. Lozano, Texas Sour Orange Juice Used in Scaffolds for Tissue Engineering, *Membranes*, 2018, **8**, 38.
45 N. S. Gundogdu, Y. Akgul and A. Kilic, Optimization of centrifugally spun thermoplastic polyurethane nanofibers for air filtration applications, *Aerosol Sci. Technol.*, 2018, **52**, 515–523.
46 C. Hernandez, S. K. Gupta, J. P. Zuniga, J. Vidal, R. Galvan, M. Martinez, H. Guzman, L. Chavez, Y. Mao and K. Lozano, Performance evaluation of Ce3+ doped flexible PVDF fibers for efficient optical pressure sensors, *Sens. Actuators, A*, 2019, **298**, 111595.
47 M. Akia, N. Salinas, S. Luna, E. Medina, A. Valdez, J. Lopez, J. Ayala, M. Alcoutlabi and K. Lozano, In situ synthesis of Fe_3O_4-reinforced carbon fiber composites as anodes in lithium-ion batteries, *J. Mater. Sci.*, 2019, **54**, 13479–13490.
48 S. K. Gupta, C. Hernandez, J. P. Zuniga, K. Lozano and Y. Mao, Luminescent PVDF nanocomposite films and fibers encapsulated with $La_2Hf_2O_7$:Eu^{3+} nanoparticles, *SN Appl. Sci.*, 2020, **2**, 1–11.
49 Y. J. Choi, D. Hwang, H. Chung, D. Y. Kim and D. Kim, Controlling the spatial distribution of quantum dots in nanofiber for light-harvesting devices, *NPG Asia Mater.*, 2015, **7**, e202.
50 C. Wang, H. Lin, Z. Zhang, Z. Qiu, H. Yang, Y. Cheng, J. Xu, X. Xiang, L. Zhang and Y. Wang, X-ray excited $CsPb(Cl,Br)_3$ perovskite quantum dots-glass composite with long-lifetime, *J. Eur. Ceram. Soc.*, 2020, **40**, 2234–2238.
51 H. Parangusan, D. Ponnamma and M. A. A. AlMaadeed, Toward High Power Generating Piezoelectric Nanofibers: Influence of Particle Size and Surface Electrostatic Interaction of Ce–Fe_2O_3 and Ce–Co_3O_4 on PVDF, *ACS Omega*, 2019, **4**, 6312–6323.
52 M. A. Hammami, M. Krifa and O. Harzallah, Centrifugal force spinning of PA6 nanofibers–processability and morphology of solution-spun fibers, *J. Text. Inst.*, 2014, **105**, 637–647.
53 Z. Bao, W. Wang, H.-Y. Tsai, H.-C. Wang, S. Chen and R.-S. Liu, Photo-/electro-luminescence enhancement of CsPbX3 (X = Cl, Br, or I) perovskite quantum dots *via* thiocyanate surface modification, *J. Mater. Chem. C*, 2020, **8**, 1065–1071.
54 E. Yassitepe, Z. Yang, O. Voznyy, Y. Kim, G. Walters, J. A. Castañeda, P. Kanjanaboos, M. Yuan, X. Gong, F. Fan, J. Pan, S. Hoogland, R. Comin, O. M. Bakr, L. A. Padilha, A. F. Nogueira and E. H. Sargent, Amine-Free Synthesis of Cesium Lead Halide Perovskite Quantum Dots for Efficient Light-Emitting Diodes, *Adv. Funct. Mater.*, 2016, **26**, 8757–8763.
55 G. Vijayakumari, N. Selvakumar, K. Jeyasubramanian and R. Mala, Investigation on the Electrical Properties of Polymer metal Nanocomposites for Physiological sensing applications, *Phys. Proc.*, 2013, **49**, 67–78.
56 Y. Song, X. Zhang, L. Li, Z. Mo, J. Xu, S. Yu, X. Liu and J. Zhang, Temperature-dependent photoluminescence of cesium lead halide perovskite (CsPbX3, X = Br, Cl, I) quantum dots, *Mater. Res. Express*, 2019, **6**, 115064.
57 C. Yu, Z. Chen, J. J. Wang, W. Pfenninger, N. Vockic, J. T. Kenney and K. Shum, Temperature dependence of

the band gap of perovskite semiconductor compound $CsSnI_3$, *J. Appl. Phys.*, 2011, **110**, 063526.

58 K. Wu, A. Bera, C. Ma, Y. Du, Y. Yang, L. Li and T. Wu, Temperature-dependent excitonic photoluminescence of hybrid organometal halide perovskite films, *Phys. Chem. Chem. Phys.*, 2014, **16**, 22476–22481.

59 Y. Hu, J. Shu, X. Zhang, A. Zhao, Y. Liu, R. Li, Y. Di, H. Xu and Z. Gan, Encapsulation of colloid perovskite nanocrystals into solid polymer matrices: Impact on electronic transition and photoluminescence, *J. Lumin.*, 2020, **219**, 116938.

60 Z. Gan, W. Chen, L. Yuan, G. Cao, C. Zhou, S. Huang, X. Wen and B. Jia, External Stokes shift of perovskite nanocrystals enlarged by photon recycling, *Appl. Phys. Lett.*, 2019, **114**, 011906.

61 Z. Gan, X. Wen, W. Chen, C. Zhou, S. Yang, G. Cao, K. P. Ghiggino, H. Zhang and B. Jia, The Dominant Energy Transport Pathway in Halide Perovskites: Photon Recycling or Carrier Diffusion?, *Adv. Energy Mater.*, 2019, **9**, 1900185.